Title

Controlling the Movement of a TRR Spatial Chain with Coupled Six-bar Function Generators for Biomimetic Motion

Permalink

Authors

Plecnik, MM
McCarthy, JM

Publication Date

2023-12-10

Peer reviewed

Controlling the Movement of a TRR Spatial Chain with Coupled Six-bar Function Generators for Biomimetic Motion

Mark M. Plecnik[*]
Robotics and Automation Laboratory
Department of Mechanical and Aerospace Engineering
University of California
Irvine, California 92697
Email: mplecnik@uci.edu

J. Michael McCarthy
Robotics and Automation Laboratory
Department of Mechanical and Aerospace Engineering
University of California
Irvine, California 92697
Email: jmmccart@uci.edu

This paper describes a synthesis technique that constrains a spatial serial chain into a single degree-of-freedom mechanism using planar six-bar function generators. The synthesis process begins by specifying the target motion of a serial chain that is parameterized by time. The goal is to create a mechanism with a constant velocity rotary input that will achieve that motion. To do this we solve the inverse kinematics equations to find functions of each serial joint angle with respect to time. Since a constant velocity input is desired, time is proportional to the angle of the input link, and each serial joint angle can be expressed as functions of the input angle. This poses a separate function generator problem to control each joint of the serial chain. Function generators are linkages that coordinate their input and output angles. Each function is synthesized using a technique that finds 11 position Stephenson II linkages, which are then packaged onto the serial chain. Using pulleys and the scaling capabilities of function generating linkages, the final device can be packaged compactly. We describe this synthesis procedure through the design of a biomimetic device for reproducing a flapping wing motion.

1 Introduction

This paper presents a procedure for constraining multi-degree-of-freedom spatial chains into single degree-of-freedom mechanisms with each joint angle controlled by a Stephenson II six-bar function generator. We choose to illustrate this method by dedicating this paper to the example design of a biomimetic device that aims to reproduce the flapping motion of a bird wing through the control of a spatial four degree-of-freedom TRR chain.

The synthesis process begins by defining the periodic motion of a TRR spatial chain by sequences of joint angles spaced at constant time steps. Joint angle data sequences are then aligned to coordinate with the motion of a fully rotatable input crank, then transformed into continuous periodic functions via Fourier series. A Fourier-based function of the input crank angle is created for each of the four serial joint angles of the TRR chain. These four input-output functions are then mechanized via the design of Stephenson II six-bar function generators. The resulting Stephenson II function generators can be packaged onto the TRR chain in manner such that their input cranks share a constant angular velocity and the motion of their output links is transmitted to the appropriate joint. The function generators can be packaged compactly onto a final device since coordinated input-output angles are maintained through stretch-rotations.

The final device creates a complex spatial movement from a constant rotary input. Since the device is timed by this input, the velocities and accelerations of the spatial chain are designed on top of its position requirements. This is evident in the wing mechanism by a slow extended downstroke and a quick contracted upstroke characteristic of the vortex ring gait.

Furthermore, since six-bar function generators are capable of achieving 11 task positions, the mechanized motion is fairly accurate to the desired motion. The synthesis equations for Stephenson II function generators capable of achieving 11 task positions are formulated below and solutions are ob-

---

[*]Address all correspondence to this author.

tained using a regeneration homotopy implemented by the polynomial solver Bertini [1, 2]. Large solution sets are generated which create several linkage design alternatives.

2 Literature Review

Equations for the design of spatial linkages that reach a finite number of positions were formulated by Roth [3, 4]. Sandor formulated spatial kinematics equations using a general quaternion-operator method [5]. Suh used displacement matrices to design RSSR linkages for rigid body guidance [6]. Tsai and Roth formulated design equations for dyads with various joints for rigid body guidance and function generation [7]. Sandor et al. formulated loop-closure equations for the synthesis of spatial motion generators comprised of various joint pairs, and provided a means for eliminating branch defects [8].

Many researchers have contributed to the field of spatial linkage design by formulating and solving equations for open serial chains including SS dyads [9–11], CC dyads [12, 13], RR dyads [14], RRR chains [15–17], PRS chains [18], RPS chains [19], RP dyads [20], and RC dyads [21]. These works construct closed loop mechanisms from open loop chains. The works of Perez et al. [22], and Perez and McCarthy [23, 24] have generalized these theories to encompass a wide variety of spatial chains. Simo-Serra and Perez-Gracia [25] have introduced a new technique of synthesizing spatial tree structures. Another approach is taken by Soh [26] who begins by specifying a six degree-of-freedom spatial chain then explores several ways to constrain it with TS chains. Our work is most like Soh in that we first specify an open serial chain, but instead of constraining it with more spatial chains we use planar function generators.

Function generators were designed by Svoboda [27] using nomographs. McLarnan [28] formulated the design equations for Stephenson II and III, and Watt II six-bar function generators and solved them with the Newton-Raphson method to obtain some solutions. Dhingra et al. [29] applied multihomogeneous homotopy method for the solution of six-bar function generators capable of reaching nine positions. Luo and Dai [30] applied a method they termed the Patterned Bootstrap method for the solution of 11 position function generators. Plecnik and McCarthy [31] applied parameter homotopy methods for the design of 11 position six-bar function generators.

Biomimetic flapping devices have seen much attention in recent years. Banala et al. [32] designed a mechanism for out-of-plane wing like motion with twist inspired by a hawk moth that employs a planar five-bar and four-bar. McDonald and Agrawal [33] designed a bio-inspired spherical four-bar for micro air-vehicles using optimization. Sreetharan et al. [34] and Teoh and Wood [35] utilize a spherical five-bar for their Mobee and Robobee designs. Aerovironment, Inc. patented technology that uses elliptical pulleys to create a hummingbird-like flapping motion, Keenon et al. [36]. The mechanical motion of insect wing folding has been studied by Haas and Wootton [37]. Our work is different because we utilize a new spatial synthesis technique and base our trajec-
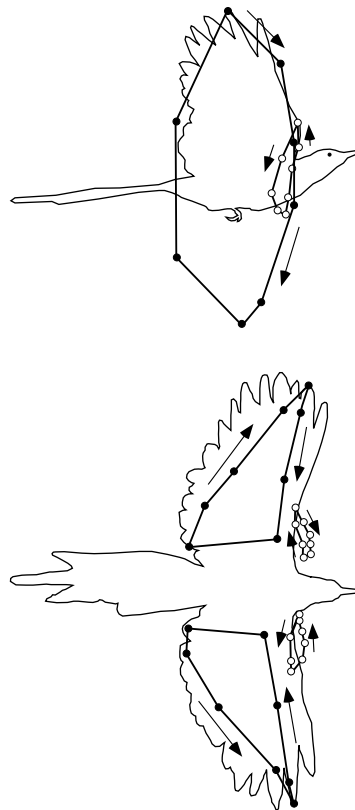

Fig. 1. This figure was reprinted from Tobalske and Dial [38] and illustrates the wing gait of an accelerating black-billed magpie

tory from data collected by [38].

3 Selection of a Spatial Chain

The goal of the example in this paper is to design a biomimetic device that recreates the wing kinematics of a black-billed magpie as documented by Tobalske and Dial [38]. They placed markers on the wrists and wingtips of these birds then recorded the frame by frame positions of these markers using high speed video for various flying conditions. The resulting data conveys information on the position and velocity of the wrist and wingtip. Tobalske and Dial conclude that the magpie selects a vortex-ring gait when accelerating that is characterized by generating lift only during the downstroke. Their data appears in Fig. 1 which is reprinted from Fig. 11 in [38]. The wrist locations are indicated by open circles and the wingtip locations are indicated by closed circles. The lateral view silhouette is in the upstroke/downstroke transition and the dorsal view silhouette is at midpoint. The time step between points is approximately constant. Our goal is to reproduce the motion documented in Fig. 1 with a constrained spatial chain.

A spatial four degree-of-freedom TRR chain is selected to represent the bones of the magpie. The T joint is placed at the shoulder and R joints are used to represent the elbow and wrist. The first axis of the T joint is perpendicular to the transverse plane of the body (along the y-axis of Fig. 2) and is measured by ψ_A. The second axis of the T joint is
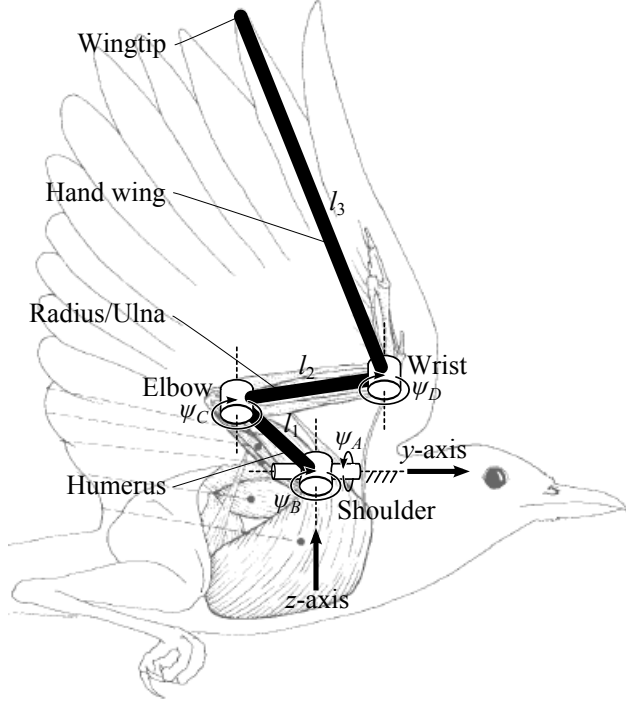
Fig. 2. The links of a TRR spatial chain correlate to the bones of a bird's wing. The magpie image is reprinted from [39]

Table 1. Coordinates of the wrist joint and the wingtip estimated from Fig. 1. The time step between points is approximately constant

Wrist	Wingtip
$\mathbf{W}_1 = \{1.79, \quad 0.80, \quad 3.55\}$	$\mathbf{V}_1 = \{5.58, \ -2.87, \quad 9.37\}$
$\mathbf{W}_2 = \{3.11, \ -0.05, \quad 1.61\}$	$\mathbf{V}_2 = \{8.97, \ -0.04, \quad 6.52\}$
$\mathbf{W}_3 = \{3.37, \ -0.61, \ -0.24\}$	$\mathbf{V}_3 = \{10.77, \quad 0.68, \quad 2.26\}$
$\mathbf{W}_4 = \{2.98, \ -0.30, \ -1.18\}$	$\mathbf{V}_4 = \{9.63, \quad 0.68, \ -1.10\}$
$\mathbf{W}_5 = \{2.10, \quad 0.14, \ -1.40\}$	$\mathbf{V}_5 = \{5.49, \ -1.08, \ -6.33\}$
$\mathbf{W}_6 = \{1.48, \quad 0.26, \ -0.46\}$	$\mathbf{V}_6 = \{1.66, \ -2.14, \ -7.49\}$
$\mathbf{W}_7 = \{0.91, \quad 0.48, \quad 1.08\}$	$\mathbf{V}_7 = \{1.35, \ -5.62, \ -3.92\}$
$\mathbf{W}_8 = \{0.57, \quad 0.89, \quad 2.24\}$	$\mathbf{V}_8 = \{2.67, \ -5.66, \quad 3.42\}$

Dual quaternion transformations are described in McCarthy and Soh [40]. Note that ψ_B, ψ_C, and ψ_D measure the angles between the fixed y-axis and the humerus, radius/ulna, and hand wing joints, respectively.

perpendicular to the plane defined by the point locations of the shoulder, elbow, and wrist joints and is measured by ψ_B. This joint is parallel to the elbow and wrist R joints which are located by distances l_1 and l_2 from the previous joint, and measured by ψ_C and ψ_D, respectively. The wingtip is a distance l_3 away from the wrist joint.

The lengths of the humerus and radius/ulna links were not measured but estimated by the authors of this paper as $l_1 = 1.8$ in and $l_2 = 2.3$ in. The length of the hand wing was obtained from the mean recorded by Tobalske and Dial of $l_3 = 7.6$ in.

The Denavit-Hartenberg convention is used to write the kinematics equations of the TRR chain,

$$\hat{D}(\psi_A, \psi_B, \psi_C, \psi_D) = \hat{X}\left(-\frac{\pi}{2}, 0\right) \hat{Z}(\psi_A, 0) \hat{X}\left(\frac{\pi}{2}, 0\right) \hat{Z}(\psi_B, 0)$$
$$\times \hat{X}(0, l_1) \hat{Z}(\psi_C - \psi_B, 0) \hat{X}(0, l_2) \hat{Z}(\psi_D - \psi_C, 0) \hat{X}(0, l_3) \tag{1}$$

where $\hat{X}$ and $\hat{Z}$ are dual quaternion transformations defined by

$$\hat{X}(\alpha, a) = \cos\frac{\alpha}{2} + \sin\frac{\alpha}{2}\begin{Bmatrix}1\\0\\0\end{Bmatrix} + \varepsilon\frac{a}{2}\left(-\sin\frac{\alpha}{2} + \cos\frac{\alpha}{2}\begin{Bmatrix}1\\0\\0\end{Bmatrix}\right)$$

$$\hat{Z}(\theta, d) = \cos\frac{\theta}{2} + \sin\frac{\theta}{2}\begin{Bmatrix}0\\0\\1\end{Bmatrix} + \varepsilon\frac{d}{2}\left(-\sin\frac{\theta}{2} + \cos\frac{\theta}{2}\begin{Bmatrix}1\\0\\0\end{Bmatrix}\right) \tag{2}$$

4 Motion of the Shoulder and Elbow Joints

The next step is to determine the motion of the spatial chain from the data gathered in Fig. 1. To do this we first determine the configurations of the shoulder-elbow TR sub-chain defined by ψ_A, ψ_B, and ψ_C from the recorded wrist positions. The two views of Fig. 1 were manually replotted into the Solidworks sketch environment in order to obtain the x, y, z coordinates of each point. This process produced inconsistencies between views which were resolved by slightly shifting some points. As well, the exact location of the shoulder joint was unknown and so needed to be estimated from the silhouettes of Fig. 1. The result of this process is a set of eight estimated point locations of the wrist that are spaced at equal time steps, Table 1.

Table 1 describes a discrete periodic trajectory. The number of points in this trajectory is increased by connecting each data point with straight lines of points spaced apart by $\Delta P = 0.05$ in . These points are expressed as,

$$\mathbf{P}_{i,j} = \mathbf{W}_i + \frac{\mathbf{W}_{i+1} - \mathbf{W}_i}{|\mathbf{W}_{i+1} - \mathbf{W}_i|}\Delta P j,$$

$$i = 1, \ldots, 8$$
$$j = 0, \ldots, l_i, \quad l_i = \max\left(\{m \mid m \in \mathbb{Z}, \Delta P m < |\mathbf{W}_{i+1} - \mathbf{W}_i|\}\right) \tag{3}$$

where $\mathbf{W}_9$ evaluates to $\mathbf{W}_1$ when $i = 8$ in order to complete the circuit. For convenience, we quickly abandon the i and j indices for a single index k so that the new discretized trajectory is $\mathbf{P}_k$ for $k = 1, \ldots, n$ where n is the number of points in
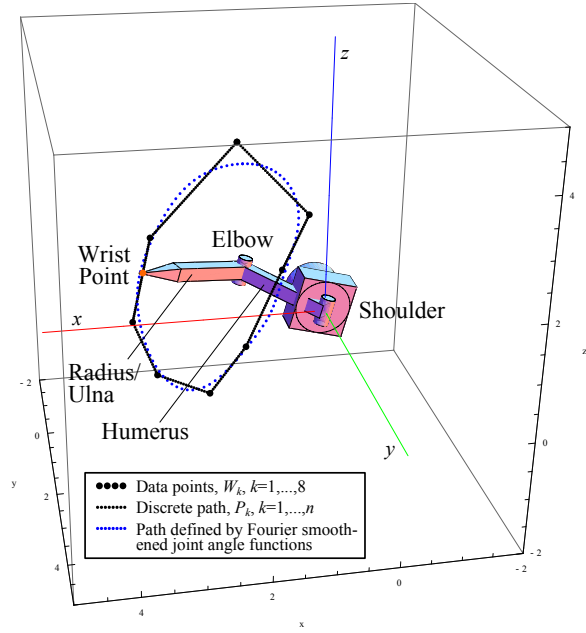
Fig. 3. The sequence of points $\mathbf{P}_k$, $k = 1, \ldots, n$ is shown in black. By fitting Fourier series to the discrete joint angle functions for ψ_A, ψ_B, ψ_C, a new smoother trajectory is generated shown in blue

the sequence described in (3). That is,

$$\mathbf{P}_k, \quad k = 1, \ldots, n, \quad \text{for} \quad n = \sum_{i=1}^{8} (l_i + 1). \tag{4}$$

Next we would like to map points $\mathbf{P}_k$ to configurations of the shoulder-elbow TR subchain by solving the inverse kinematics. The shoulder-elbow TR subchain is a three degree-of-freedom linkage that is fully determined when the point location of the wrist joint is specified. To solve the inverse kinematics, we separate out the first portion of the Denavit-Hartenberg equations (1) that pertain to the TR subchain

$$\hat{D}_{TR}(\psi_A, \psi_B, \psi_C) = \hat{X}(-\frac{\pi}{2}, 0)\hat{Z}(\psi_A, 0)\hat{X}(\frac{\pi}{2}, 0)\hat{Z}(\psi_B, 0)$$
$$\times \hat{X}(0, l_1)\hat{Z}(\psi_C - \psi_B, 0)\hat{X}(0, l_2) \tag{5}$$

$\hat{D}_{TR}$ is a transformation that represents a translation to the point location of the wrist and a rotation that aligns with the radius/ulna link. $\hat{D}_{TR}$ expands to

$$\hat{D}_{TR} = h_0 + h_1 \varepsilon \tag{6}$$

where h_0 and h_1 are the primal and dual parts, respectively,

and evaluate to

$$h_0 = \cos\frac{\psi_A}{2}\cos\frac{\psi_C}{2} + \left\{ \begin{array}{c} \sin\frac{\psi_A}{2}\sin\frac{\psi_C}{2} \\ \sin\frac{\psi_A}{2}\cos\frac{\psi_C}{2} \\ \cos\frac{\psi_A}{2}\sin\frac{\psi_C}{2} \end{array} \right\}$$

$$h_1 = -\frac{1}{2}\sin\frac{\psi_A}{2}\left(l_1\sin\left(\psi_B - \frac{\psi_C}{2}\right) + l_2\sin\frac{\psi_C}{2}\right)$$
$$+ \frac{1}{2}\left\{ \begin{array}{c} \cos\frac{\psi_A}{2}\left(l_1\cos\left(\psi_B - \frac{\psi_C}{2}\right) + l_2\cos\frac{\psi_C}{2}\right) \\ \cos\frac{\psi_A}{2}\left(l_1\sin\left(\psi_B - \frac{\psi_C}{2}\right) + l_2\sin\frac{\psi_C}{2}\right) \\ -\sin\frac{\psi_A}{2}\left(l_1\cos\left(\psi_B - \frac{\psi_C}{2}\right) + l_2\cos\frac{\psi_C}{2}\right) \end{array} \right\} \tag{7}$$

The translation vector $\mathbf{P}$ of this transformation can be extracted by the relation

$$\mathbf{P} = \left\{ \begin{array}{c} P_x \\ P_y \\ P_z \end{array} \right\} = 2h_1 h_0^* \tag{8}$$

where h_0^* is the quaternion conjugate of h_0. We expand $\mathbf{P}$ to obtain the inverse kinematics equations,

$$P_x = \cos\psi_A(l_1\cos\psi_B + l_2\cos\psi_C) \tag{9}$$
$$P_y = l_1\sin\psi_B + l_2\sin\psi_C \tag{10}$$
$$P_z = -\sin\psi_A(l_1\cos\psi_B + l_2\cos\psi_C) \tag{11}$$

For the inverse kinematics, the wrist location $\{P_x, P_y, P_z\}$ is specified and joint angles ψ_A, ψ_B, ψ_C are solved for. The unknown ψ_A is found by dividing (11) by (9) and taking the arctan function,

$$\psi_A = \arctan\frac{-P_z}{P_x} \tag{12}$$

In order to find ψ_B, we rearrange (9) and (10),

$$l_2\cos\psi_C = P_x\sec\psi_A - l_1\cos\psi_B \tag{13}$$
$$l_2\sin\psi_C = P_y - l_1\sin\psi_B \tag{14}$$

then square and add (13) and (14) to eliminate ψ_C and obtain

$$l_2^2 = (p_x\sec\psi_A - l_1\cos\psi_B)^2 + (p_y - l_1\sin\psi_B)^2. \tag{15}$$

The identity

$$\sec\psi_A = \frac{\sqrt{P_z^2 + P_x^2}}{P_x} \tag{16}$$

can be found from Eqn. (12) and is substituted into the expanded version of (15) to obtain

$$2l_1\sqrt{P_z^2 + P_x^2}\cos\psi_B + 2P_y l_1\sin\psi_B - P_x^2 - P_y^2 - P_z^2 - l_1^2 + l_2^2 = 0 \tag{17}$$

(a) Joint angle ψ_A

(b) Joint angle ψ_B

(c) Joint angle ψ_C

(d) Joint angle ψ_D

.... Discrete trajectory   ●●●● Specified Task Points

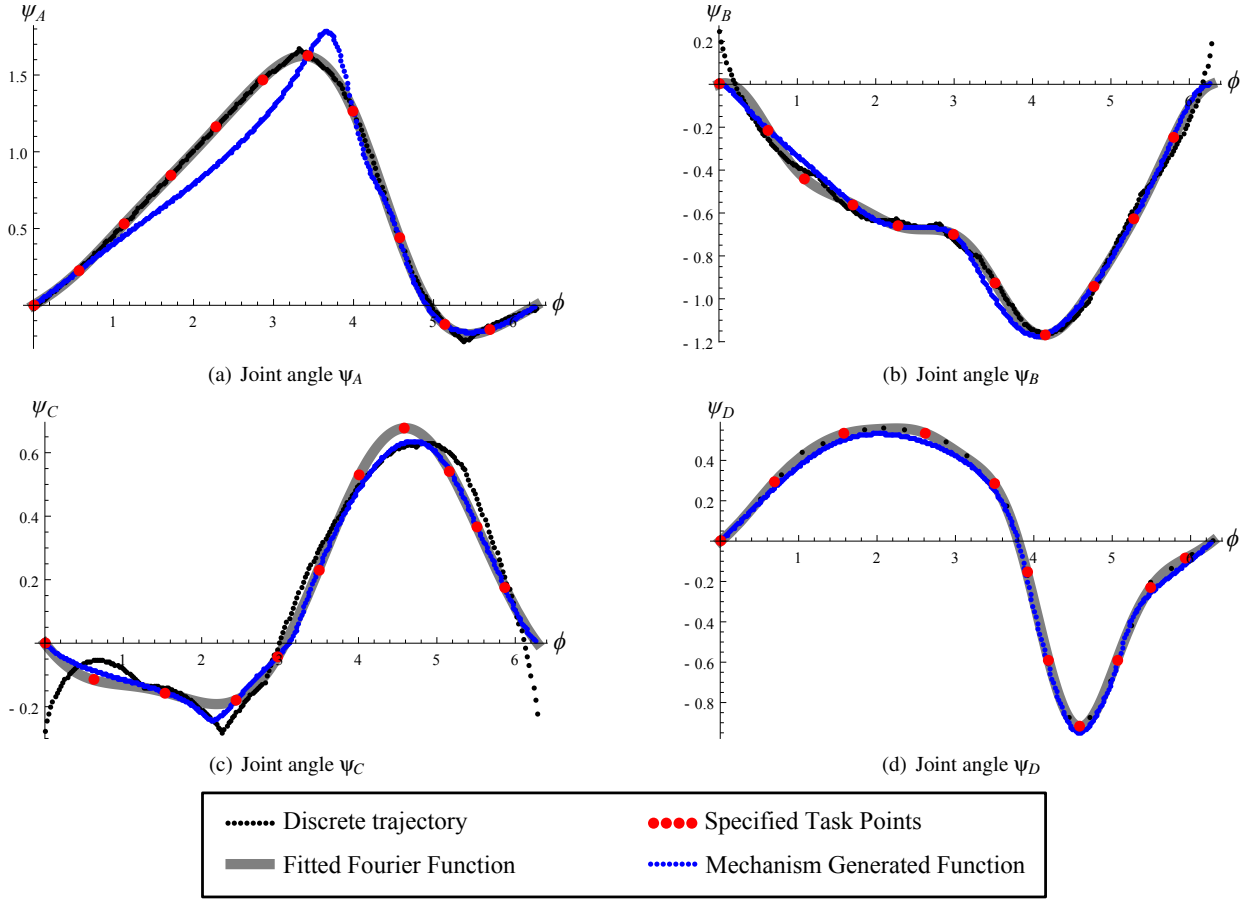━━━ Fitted Fourier Function   .... Mechanism Generated Function

Fig. 4. The discrete data curves (black) were fitted with Fourier series functions (gray). Eleven task points (red) were chosen from the Fourier functions to synthesize a mechanism (blue)

Eqn. (17) takes the form

$$A_{\text{const}} \cos \psi_B + B_{\text{const}} \sin \psi_B + C_{\text{const}} = 0 \qquad (18)$$

of which the two solutions are known to be

$$\psi_B^{\pm} = \arctan \frac{B_{\text{const}}}{A_{\text{const}}} \pm \arccos \left(\frac{-C_{\text{const}}}{\sqrt{A_{\text{const}}^2 + B_{\text{const}}^2}} \right) \qquad (19)$$

By dividing (14) by (13) and taking the arctan function, we obtain two corresponding solutions for ψ_C,

$$\psi_C^{\pm} = \arctan \left(\frac{P_y - l_1 \sin \psi_B^{\pm}}{\sqrt{P_x^2 + P_z^2} - l_1 \cos \psi_B^{\pm}} \right) \qquad (20)$$

Equations (12), (19), and (20) are the inverse kinematics solutions that describe two configurations of a TR subchain that locates the wrist point at **P**. The inverse kinematics are solved for all points $\mathbf{P}_k$ of (4) to obtain two configurations of the TR chain at each point of the discretized trajectory. The "+" configurations were dropped as they placed the bird's elbow in an unnatural location. The resulting sequence of

TR subchain configurations,

$$\{\psi_A, \psi_B^-, \psi_C^-\}_k, \quad k = 1, \ldots, n, \qquad (21)$$

represents a periodic mechanism trajectory.

5 Fitting Trajectories with Fourier Series

Next, we create another sequence of equal length,

$$\phi_k = \frac{2\pi}{n-1}(k-1), \quad k = 1, \ldots, n, \qquad (22)$$

that represents the equally spaced angles of one rotation of the input crank. Sequences (21) and (22) are paired so as to create discrete representations of joint angles ψ_A, ψ_B, ψ_C as functions of the input crank angle ϕ.

$$\{\phi, \psi_A\}_k, \quad \{\phi, \psi_B\}_k, \quad \{\phi, \psi_C\}_k, \quad k = 1, \ldots, n \qquad (23)$$

The discrete functions are then approximated with Fourier series to create continuous periodic input-output functions. As well, Fourier series serve to smooth out the discrete data curves, Fig 4. The discrete version of the Fourier

Table 2. Fourier coefficients for the joint angle functions shown in Fig. 4

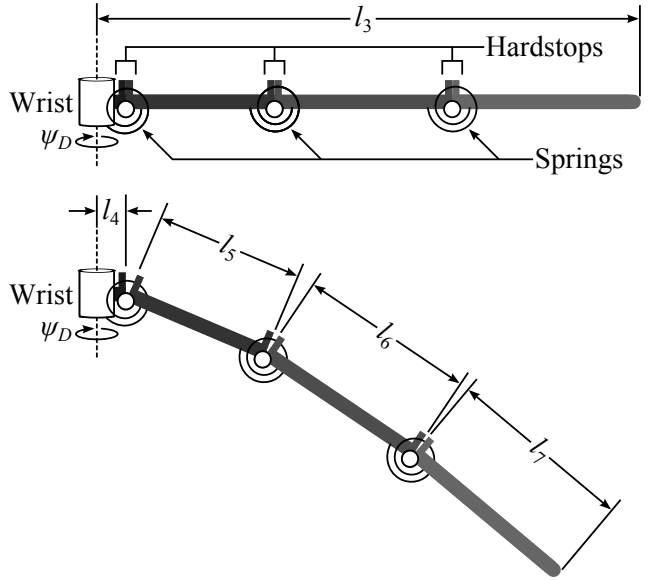|	$\psi_A = f_A(\phi)$	$\psi_B = f_B(\phi)$	$\psi_C = f_C(\phi)$	$\psi_D = f_D(\phi)$
o	4	4	2	6
a_0	−0.418185	−0.818013	0.743278	−0.280661
a_1	−0.820203	0.364468	−0.017921	−0.151247
b_1	0.197223	0.224286	−0.414395	0.583401
a_2	0.143329	0.193916	−0.119443	0.195403
b_2	0.166381	−0.072155	0.043389	−0.050086
a_3	0.026043	0.004051	0	−0.075214
b_3	−0.062797	0.003374	0	−0.115771
a_4	−0.011122	0.041918	0	−0.053983
b_4	−0.007510	0.011844	0	0.039339
a_5	0	0	0	0.020929
b_5	0	0	0	0.010725
a_6	0	0	0	−0.002909
b_6	0	0	0	−0.005818

Fig. 5. The addition of sprung joints creates a compliant hand wing design. Hard stops prevent dorsal flexure of the hand wing. The new segment lengths are $l_4 = 0.375$, $l_5 = 2.125$, $l_6 = 2.5$, AND $l_7 = 2.6$

series for a set of data points $(x,y)_k$, $k = 1,\ldots,n$ spaced over the interval $[c,d]$ is

$$f(x) = \frac{1}{2}a_0 + \sum_{m=1}^{o} (a_m \cos(\lambda_m x) + b_m \sin(\lambda_m x))$$

where $\lambda_m = \dfrac{2\pi m}{d-c}$ $\quad m = 0,1,2,\ldots$

$$a_m = \frac{2}{d-c} \sum_{k=1}^{n} (y_k \cos(\lambda_m x_k)\Delta x_k), \quad m = 0,1,2,\ldots$$

$$b_m = \frac{2}{d-c} \sum_{k=1}^{n} (y_k \sin(\lambda_m x_k)\Delta x_k), \quad m = 1,2,\ldots$$

(24)

and where o is the order of the Fourier series. For the case $(x,y)_k = (\phi,\psi)_k$, $\Delta x_k = \frac{d-c}{n-1}$, and $[c,d] = [0,2\pi]$, Eqn. (24) simplifies to

$$f(\phi) = \frac{1}{2}a_0 + \sum_{m=1}^{o} (a_m \cos(m\phi) + b_m \sin(m\phi))$$

where $a_m = \dfrac{2}{n-1} \sum_{k=1}^{n} (\psi_k \cos(m\phi_k)), \quad m = 0,1,2,\ldots$

$$b_m = \frac{2}{n-1} \sum_{k=1}^{n} (\psi_k \sin(m\phi_k)), \quad m = 1,2,\ldots$$

(25)

More information of Fourier series is found in Greenberg [41]. The discrete functions in (23) were approximated with Fourier series to obtain

$$\psi_A = f_A(\phi), \quad \psi_B = f_B(\phi), \quad \psi_C = f_C(\phi). \quad (26)$$

where the Fourier coefficients of these functions appear in Table 2. The functions of (26) represent the trajectory of the three degree-of-freedom shoulder-elbow TR subchain that we will design for.

6 Motion of the Wrist Joint

To define the trajectory of the entire TRR chain we must specify wrist joint angles, ψ_D, that control the orientations of the hand wing link. The hand wing link approximates several distal wing bones that move with respect to each other including the radiale, ulnare, carpometacarpus, and phalanges as well as the flight feathers, see Proctor [42]. We grossly take into account the movement of these bones and feathers by relaxing the length l_3 and making the hand wing link flexible. We design compliance into the hand wing by creating sprung joints limited by hard stops to prevent the wing from flexing dorsally beyond a flat configuration as shown in Fig. 5. Using this compliant hand wing design in conjunction with Solidworks Motion Analysis rigid body dynamics simulator, the function $\psi_D = f_D(\phi)$ was manually shaped to pass the wingtip closely by the points V_i, $i = 1,\ldots,8$ listed in Table 1. The manually chosen points, Table 3, were fitted with a Fourier function of which the coefficients are listed in Table 2.

Table 3. Manualy chosen values for wrist joint angle ψ_D

| ϕ	ψ_D	ϕ	ψ_D
0	-0.346448	3.141593	0.072431
0.261799	-0.241728	3.403392	-0.049742
0.523599	-0.137008	3.665191	-0.171915
0.785398	-0.023562	3.926991	-0.520981
1.047198	0.089884	4.188790	-0.957313
1.308997	0.133518	4.450590	-1.219112
1.570796	0.177151	4.712389	-1.219112
1.832596	0.207381	4.974188	-1.044580
2.094395	0.212058	5.235988	-0.765327
2.356194	0.207381	5.497787	-0.555887
2.617994	0.177151	5.759587	-0.486074
2.879793	0.142244	6.021386	-0.416261
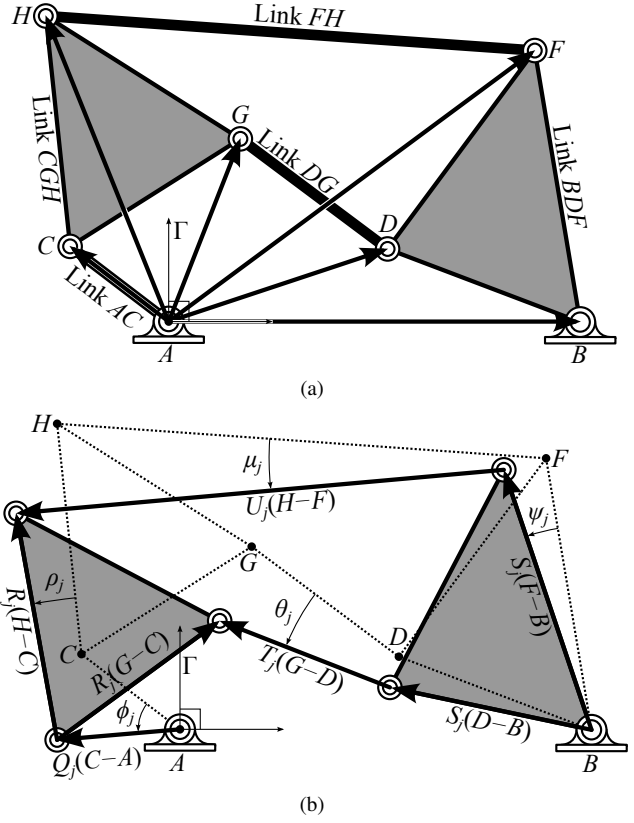
Fig. 6. A Stephenson II function generator in (a) the initial configuration and (b) the jth configuration

7 Formulation of Synthesis Equations

The goal of this section is to mechanize the functions $\psi_A = f_A(\phi)$, $\psi_B = f_B(\phi)$, $\psi_C = f_C(\phi)$, and $\psi_D = f_D(\phi)$. This is accomplished by synthesizing a Stephenson II six-bar function generator, Fig. 6, for each function. The synthesis formulation and solution is described in more depth in Plecnik and McCarthy [31].

A Stephenson II consists of five moving links named Link AC, Link BDF, Link CGH, Link DG, and Link FH. The objective is to coordinate the rotations between ϕ and ψ of Link AC and Link BDF, respectively. In general, a Stephenson II function generator can coordinate exactly 11 input-output angle pairs. In order to set the scale, orientation, and location of the linkage, the ground pivots A and B are chosen to be at $\mathbf{A} = \{0,0\}$ and $\mathbf{B} = \{1,0\}$. However, for this planar synthesis procedure we will use complex numbers to represent vectors, therefore we locate the ground pivots at $A = 0 + i0$ and $B = 1 + i0$.

Formulation of the synthesis equations begins by constructing the loop closure equations. From Fig. 6(b), we construct two sets of loop closure equations,

$$A - B + Q_j(C-A) + R_j(G-C) - S_j(D-B) - T_j(G-D) = 0, \tag{27}$$

$$A - B + Q_j(C-A) + R_j(H-C) - S_j(F-B) - U_j(H-F) = 0, \tag{28}$$

$$j = 1,\ldots,10,$$

and two sets of conjugate loop equations,

$$\bar{A} - \bar{B} + \bar{Q}_j(\bar{C}-\bar{A}) + \bar{R}_j(\bar{G}-\bar{C}) - \bar{S}_j(\bar{D}-\bar{B}) - \bar{T}_j(\bar{G}-\bar{D}) = 0, \tag{29}$$

$$\bar{A} - \bar{B} + \bar{Q}_j(\bar{C}-\bar{A}) + \bar{R}_j(\bar{H}-\bar{C}) - \bar{S}_j(\bar{F}-\bar{B}) - \bar{U}_j(\bar{H}-\bar{F}) = 0, \tag{30}$$

$$j = 1,\ldots,10,$$

where j indexes displacements of each task position from an unknown initial configuration. Note that j terminates at 10 for 11 position synthesis because the initial configuration corresponds to the task position $(\phi,\psi) = (0,0)$, without loss of generality. These equations contain the complex rotation operators Q_j, R_j, S_j, T_j, U_j, and their conjugates defined as

$$\begin{aligned} Q_j &= e^{i\phi_j}, & R_j &= e^{i\rho_j}, & S_j &= e^{i\psi_j}, \\ \bar{Q}_j &= e^{-i\phi_j}, & \bar{R}_j &= e^{-i\rho_j}, & \bar{S}_j &= e^{-i\psi_j}. \\ T_j &= e^{i\theta_j}, & U_j &= e^{i\mu_j}, \\ \bar{T}_j &= e^{-i\theta_j}, & \bar{U}_j &= e^{-i\mu_j}. \end{aligned} \tag{31}$$

The variables Q_j, $\bar{Q}_j$, S_j and $\bar{S}_j$ specify the task. The variables R_j, $\bar{R}_j$, T_j, $\bar{T}_j$, U_j, and $\bar{U}_j$ remain as unknowns. In order for these unknowns to correspond to rotational operators, it

is necessary that they satisfy the normalization conditions,

$$R_j \bar{R}_j = 1, \tag{32}$$
$$T_j \bar{T}_j = 1, \tag{33}$$
$$U_j \bar{U}_j = 1, \quad j = 1, \dots, 10. \tag{34}$$

Eqns. (27)–(30) and (32)–(34) comprise a system of 70 equations and unknowns. The unknowns of these equations are

$$\langle C, \bar{C}, D, \bar{D}, F, \bar{F}, G, \bar{G}, H, \bar{H} \rangle \text{ and } \langle R_j, \bar{R}_j, T_j, \bar{T}_j, \bar{U}_j, U_j, \rangle,$$
$$j = 1, \dots, 10. \tag{35}$$

In order to reduce the system, the unknowns T_j and $\bar{T}_j$ are eliminated by substituting Equations (27) and (29) into (33) to obtain

$$(A - B + Q_j(C - A) - S_j(D - B) + R_j(G - C))$$
$$\times (\bar{A} - \bar{B} + \bar{Q}_j(\bar{C} - \bar{A}) - \bar{S}_j(\bar{D} - \bar{B}) + \bar{R}_j(\bar{G} - \bar{C}))$$
$$= (G - D)(\bar{G} - \bar{D}) \tag{36}$$

Similarly, U_j and $\bar{U}_j$ are eliminated by substituting Equations (28) and (30) into (34) to obtain

$$(A - B + Q_j(C - A) - S_j(F - B) + R_j(H - C))$$
$$\times (\bar{A} - \bar{B} + \bar{Q}_j(\bar{C} - \bar{A}) - \bar{S}_j(\bar{F} - \bar{B}) + \bar{R}_j(\bar{H} - \bar{C}))$$
$$= (H - F)(\bar{H} - \bar{F}) \tag{37}$$

Equations (36) and (37) are expanded and written in matrix form

$$\begin{bmatrix} a\bar{b}_j & \bar{a}b_j \\ c\bar{d}_j & \bar{c}d_j \end{bmatrix} \begin{Bmatrix} R_j \\ \bar{R}_j \end{Bmatrix} = \begin{Bmatrix} f\bar{f} - a\bar{a} - b_j\bar{b}_j \\ g\bar{g} - a\bar{a} - d_j\bar{d}_j \end{Bmatrix} \tag{38}$$

where

$$a = G - C, \quad b_j = A - B + Q_j(C - A) - S_j(D - B),$$
$$c = H - C, \quad d_j = A - B + Q_j(C - A) - S_j(F - B),$$
$$f = G - D, \quad g = H - F. \tag{39}$$

Solving (38) for R_j and $\bar{R}_j$, substituting into (32), clearing the denominator, and factoring, we obtain,

$$\mathbf{a}^T \bar{\mathbf{b}}_j \mathbf{b}_j^T \bar{\mathbf{a}} - \mathbf{c}^T \bar{\mathbf{d}}_j \mathbf{d}_j^T \bar{\mathbf{c}} = 0, \quad j = 1, \dots, 10 \tag{40}$$

Table 4. Characterization of solutions and computation times for the ψ_A, ψ_B, ψ_C, and ψ_D functions

	ψ_A	ψ_B	ψ_C	ψ_D
Linkage solutions	11,428	7,215	12,870	11,693
Design candidates	6,068	4,012	7,363	5,775
11-point mechanisms	0	0	3	0
10-point mechanisms	0	0	12	0
9-point mechanisms	0	7	95	4
8-point mechanisms	21	54	246	95
7-point mechanisms	172	213	603	184
6-point mechanisms	623	364	1,349	499
Synthesis computation time (hr)	2.2	2.0	2.5	2.2
Analysis computation time (hr)	20.2	13.4	25.6	19.1

where

$$\mathbf{a} = \begin{Bmatrix} a(g\bar{g} - c\bar{c}) \\ c(f\bar{f} - a\bar{a}) \\ a \\ c \end{Bmatrix}, \quad \mathbf{b}_j = \begin{Bmatrix} b_j \\ -d_j \\ -b_j d_j \bar{d}_j \\ b_j \bar{b}_j d_j \end{Bmatrix},$$

$$\mathbf{c} = \begin{Bmatrix} a\bar{c} \\ \bar{a}c \end{Bmatrix}, \quad \mathbf{d}_j = \begin{Bmatrix} b_j \bar{d}_j \\ -\bar{b}_j d_j \end{Bmatrix}. \tag{41}$$
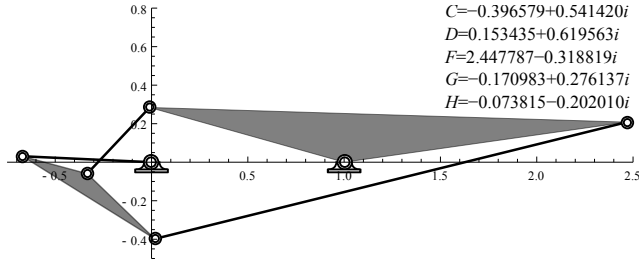
The degree of Eqn. (40) is $8^{10} \approx 1.07 \times 10^9$. Performing a multihomogeneous root count with the variable groups,

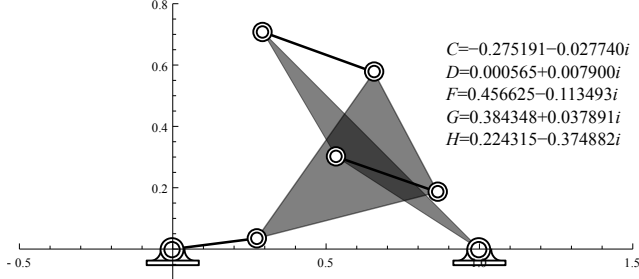$$\langle C, D, F, G, H \rangle, \quad \langle \bar{C}, \bar{D}, \bar{F}, \bar{G}, \bar{H} \rangle, \tag{42}$$

determines a reduced Bézout number of 264,241,152. This was determined by computing the coefficient in front of the monomial $\alpha_1^5 \alpha_2^5$ in the polynomial $(4\alpha_1 + 4\alpha_2)^{10}$.
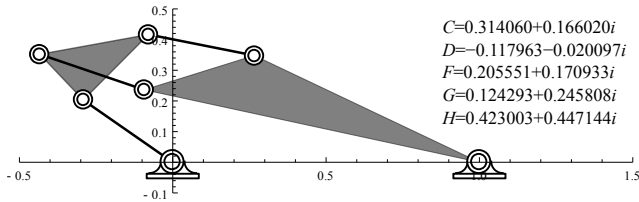
8 Solution of Synthesis Equations

A general form of Eqns. (40) was solved utilizing a regeneration homotopy implemented by the Bertini homotopy software [1, 2]. This general form consisted of specifying (Q_j, S_j), $j = 1, \dots, 10$ as random complex numbers near unity and $(\bar{Q}_j, \bar{S}_j)$, $j = 1, \dots, 10$ as the conjugates of those complex numbers. The computation took 311 hrs on 256 cores processing at 2.2 GHz. The regeneration homotopy tracked 24,822,328 paths over 10 levels to find 1,521,037 nonsingular solutions. Solutions to the general form can be used to construct parameter homotopies for efficient generation of specific solution sets. Parameter homotopies were
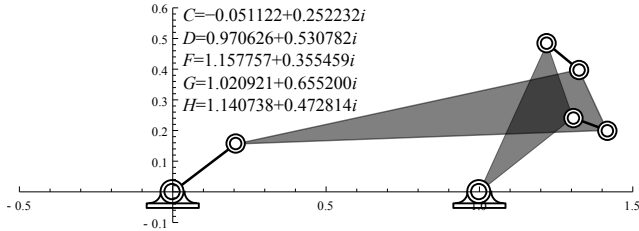
(a) Mechanism for $\psi_A = f_A(\phi)$ that passes through 7 task positions

$C=-0.396579+0.541420i$
$D=0.153435+0.619563i$
$F=2.447787-0.318819i$
$G=-0.170983+0.276137i$
$H=-0.073815-0.202010i$

(b) Mechanism for $\psi_B = f_B(\phi)$ that passes through 9 task positions

$C=-0.275191-0.027740i$
$D=0.000565+0.007900i$
$F=0.456625-0.113493i$
$G=0.384348+0.037891i$
$H=0.224315-0.374882i$

(c) Mechanism for $\psi_C = f_C(\phi)$ that passes through 8 task positions

$C=0.314060+0.166020i$
$D=-0.117963-0.020097i$
$F=0.205551+0.170933i$
$G=0.124293+0.245808i$
$H=0.423003+0.447144i$

$C=-0.051122+0.252232i$
$D=0.970626+0.530782i$
$F=1.157757+0.355459i$
$G=1.020921+0.655200i$
$H=1.140738+0.472814i$

(d) Mechanism for $\psi_D = f_D(\phi)$ that passes through 9 task positions

Fig. 7. The four linkage solutions which were selected to mechanize the magpie wing trajectory. All linkages possess a fully rotatable input crank

used to solve the synthesis equations for the four function generators desired in this paper.

Table 4 lists the number of linkage solutions for each desired function and the computation time required to find and analyze those solutions. Linkage solutions refers to non-singular solutions in which unknowns and their overbarred counterparts, i.e. C and $\bar{C}$, are indeed conjugate so as to describe physical point locations. Design candidates excludes redundant solution pairs and includes additional cognate linkages that were not found through the homotopy solution which is discussed further below. Linkages counted as 11-point mechanisms are those that achieve 11 task positions on a single trajectory without encountering a singular configuration, and so forth for 10-, 9-, 8-, 7-, 6-point mechanisms. Synthesis computation time was how long the Bertini parameter homotopy took to execute. Analysis computation
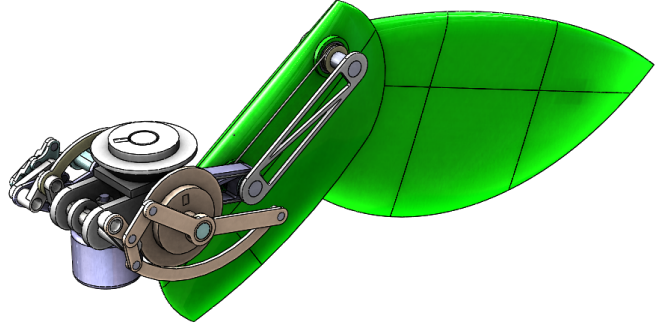

Fig. 8. A prototype design for the function generator controlled magpie wing

time was how long it took to solve the forward kinematics, sort those solutions into trajectories, and count how many task points each trajectory passed through. For more details on the analysis process, see Plecnik and McCarthy [31].

Homotopy algorithms are capable of finding entire solution sets for large polynomial systems. However, due to highly nonlinear synthesis equations and the numerical nature of homotopy, our solution sets have been found to be incomplete as additional solutions have been discovered. In particular, the symmetry of the Stephenson II mechanism requires that for every solution

$$\{C, D, F, G, H, \bar{C}, \bar{D}, \bar{F}, \bar{G}, \bar{H}\} \qquad (43)$$

there should exist another solution where the values of $\{D, \bar{D}\}$ and $\{F, \bar{F}\}$, and the values of $\{G, \bar{G}\}$ and $\{H, \bar{H}\}$, are interchanged, yet all these pairs are not found. Both of these solutions describe the same linkage geometry so we term them redundant. Furthermore, Dijksman [43] details that Stephenson II function generators come in cognate triples, and in our solution sets we find instances of incomplete cognate sets. Therefore, for each set of linkage solutions we remove one member of each redundant pair and generate any missing cognates before we begin the analysis procedure.

The objective of the analysis procedure is to find mechanism trajectories that achieve all task positions in the absence of singularities. The percentage of linkage solutions that are capable of producing these trajectories is usually low. However, we find that mechanism trajectories which produce almost all 11 task positions are still practically useful. Therefore, we keep track of these mechanisms in Table 4. None of the linkages chosen to mechanize the magpie trajectory in this paper actually achieved all 11 positions in a single mechanism trajectory. The four function generators that were chosen to mechanize $\psi_A = f_A(\phi)$, $\psi_B = f_B(\phi)$, $\psi_C = f_C(\phi)$, $\psi_D = f_D(\phi)$ are shown in Fig. 7. The functions produced by the chosen mechanisms are plotted in Fig. 4.

9 Results

The four linkages shown in Fig. 7 can be packaged onto the spatial TRR chain of Fig. 2 such that all four function
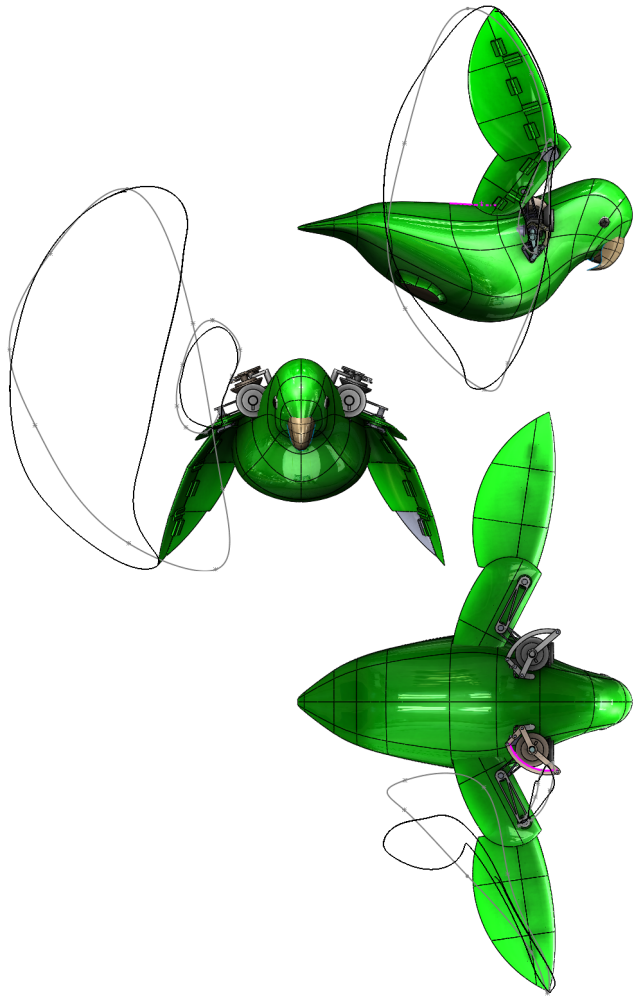
Fig. 9. The wingtip path (black) of the function generator controlled magpie wing alongside the desired path (gray) interpretted from the data recorded in Fig. 1

generators are driven by the same input crank and the motion of the output links are transmitted to the proper controlled joint. An embodiment of this idea is shown in Fig. 8. Since function generators can be scaled while maintaining the same input-output angles, the four function generators are made compact and mounted close to the motor. The shoulder motion of ψ_A is transmitted through a pair of bevel gears and the elbow and wrist motions of ψ_C and ψ_D are transmitted through pulleys. The shoulder motion of ψ_B is directly driven. A video of this prototype design can be found at http://sites.uci.edu/markplecnik/projects/wing-mechanism/ .

The wingtip path of the prototype design was generated using Solidworks Motion Analysis rigid body dynamics simulator. It is shown compared to the target trajectory in Fig. 9. The lateral view shows the wing at the upstroke to downstroke transition. The cephalad view shows the wing at the downstroke to upstroke transition. The dorsal view shows the wing at mid downstroke.

10 Conclusion

This paper demonstrates how to constrain a mutli-degree-of-freedom spatial TRR chain to a complex single degree-of-freedom mechanism controlled by Stephenson II six-bar function generators. This process included defining the target motion as discrete data, computing trajectories of joint angles, fitting discrete trajectories with smooth continuous periodic functions using Fourier series, synthesizing an 11 position Stephenson II function generator for each joint angle function, then packaging the function generators onto the TRR chain such that the input cranks share an angular velocity and the output links transmit motion to their corresponding joints.

The synthesis equations for Stephenson II six-bar function generators capable of achieving 11 positions were formulated and solved. The polynomial solver Bertini was used to solve the system generally with a regeneration homotopy which was then used to solve specific systems with parameter homotopies. The solution sets provided a large set of linkages of which a small percentage were useful. Four useful mechanisms were chosen to be designed onto a prototype wing flapping mechanism. The resulting wing trajectory approximates the data recorded by Tobalske and Dial [38].

References

[1] D. J. Bates, J. D. Hauenstein, A. J. Sommese, and C. W. Wampler. *Bertini: Software for Numerical Algebraic Geometry*. Available at bertini.nd.edu with permanent doi: dx.doi.org/10.7274/R0H41PB5.

[2] D. J. Bates, J. D. Hauenstein, A. J. Sommese, and C. W. Wampler, 2013. *Numerically Solving Polynomial Systems with Bertini*, SIAM Press, Philadelphia.

[3] B. Roth, 1967. "The kinematics of motion through finitely separated positions," *Journal of Applied Mechanics*, 34(3):591–598.

[4] B. Roth, 1967. "Finite-position theory applied to mechanism synthesis," *Journal of Applied Mechanics*, 34(3):599–605.

[5] G. N. Sandor, 1968. "Principles of a general quaternion-operator method of spatial kinematic synthesis," *Journal of Applied Mechanics*, 35(1):40–46.

[6] C. H. Suh, 1968. "Design of space mechanisms for rigid body guidance," *Journal of Manufacturing Science and Engineering*, 90(3):499–506.

[7] L. W. Tsai and B. Roth, 1972. "Design of dyads with helical, cylindrical, spherical, revolute and prismatic joints," *Mechanism and Machine Theory*, 7(1):85–102.

[8] G. N. Sandor, T. Weng, and Y. Xu, 1988. "The synthesis of spatial motion generators with prismatic, revolute and cylindric pairs without branching defect," *Mechanism and Machine Theory*, 23(4):269–274.

[9] C. Innocenti, 1995. "Polynomial solution of the spatial Burmester problem," *Journal of Mechanical Design* 117(1):64–68.

[10] Q. Liao, and J. M. McCarthy, 2001. "On the seven position synthesis of a 5-SS platform linkage," *Journal of Mechanical Design* 123(1):74–79.

[11] M. Plecnik and J. M. McCarthy, 2012. "Design of a 5-SS spatial steering linkage," *Proceedings of the ASME 2012 IDETC/CIE Conference*, Paper No. DETC2012-71405, August 12–15, 2012, Chicago, USA.

[12] A. P. Murray and J. M. McCarthy, 1999. "Burmester lines of spatial five position synthesis from the analysis of a 3-CPC platform," *Journal of Mechanical Design*, 121(1):45–49.

[13] P. Larochelle, 2012. "Synthesis of Spatial CC Dyads and 4C Mechanisms for Pick & Place Tasks With Guiding Locations," *Latest Advances in Robot Kinematics*, Springer Netherlands, 437–444.

[14] C. Mavroidis, E. Lee, and M. Alam, 2001. "A New Polynomial Solution to the Geometric Design Problem of Spatial RR Robot Manipulators Using the Denavit and Hartenberg Parameters," *Journal of Mechanical Design*, 123(1): 58–67.

[15] E. Lee, C. Mavroidis, and J. P. Merlet, 2002. "Five precision points synthesis of spatial RRR manipulators using interval analysis," *Proceedings of the ASME 2002 IDETC/CIE Conference*, Paper No. DETC2002/MECH-34272, September 29–October 2, 2002, Montreal, Canada.

[16] E. Lee and C. Mavroidis, 2002. "Solving the geometric design problem of spatial 3R robot manipulators using polynomial homotopy continuation," *Journal of Mechanical Design*, 124(4):652–661.

[17] E. Lee and C. Mavroidis, 2004. "Geometric design of 3r robot manipulators for reaching four end-effector spatial poses," *The International Journal of Robotics Research*, 23(3):247–254.

[18] H. Su, C. W. Wampler, and J. M. McCarthy, 2004. "Geometric design of cylindric PRS serial chains," *Journal of Mechanical Design*, 126(2):269–277.

[19] H. Su and J. M. McCarthy, 2005, 2005. "The synthesis of an RPS serial chain to reach a given set of task positions," *Mechanism and Machine Theory*, 40(7):757–775.

[20] A. Perez-Gracia, 2011. "Synthesis of spatial RPRP closed linkages for a given screw system," *Journal of Mechanisms and Robotics*, 3(2):021009.

[21] B. Batbold, Y. Yihun, J. S. Wolper, and A. Perez-Gracia, 2014. "Exact Workspace Synthesis for RCCR Linkages," *Computational Kinematics*, Springer Netherlands, 349–357.

[22] A. Perez and J. M. McCarthy, 2004. "Dual quaternion synthesis of constrained robotic systems," *Journal of Mechanical Design*, 126(3):425–435.

[23] A. Perez, H. Su, and J. M. McCarthy, 2004. "Synthetica 2.0: software for the synthesis of constrained serial chains," *Proceedings of the ASME 2004 IDETC/CIE Conference*, Paper No. DETC2004-57524, September 28–October 2, 2004, Salt Lake City, USA.

[24] A. Perez-Gracia and J. M. McCarthy, 2006. "Kinematic synthesis of spatial serial chains using Clifford algebra exponentials," *Proceedings of the Institution of Mechanical Engineers, Part C: Journal of Mechanical Engineering Science*, 220(7):953–968.

[25] E. Simo-Serra and A. Perez-Gracia, 2014. "Kinematic synthesis using tree topologies," *Mechanism and Machine Theory*, 72:94–113.

[26] G. S. Soh, 2014. "Rigid Body Guidance of Human Gait as Constrained TRS Serial Chain," *Proceedings of the ASME 2014 IDETC/CIE Conference*, Paper No. DETC2014-34881, August 17–20, 2014, Buffalo, New York, USA.

[27] A. Svoboda, 1948. *Computing Mechanisms and Linkages*, McGraw-Hill, New York, NY.

[28] C. W. McLarnan, 1963. "Synthesis of six-link plane mechanisms by numerical analysis," *Journal of Engineering for Industry*, 85(1):5–10.

[29] A. K. Dhingra, J. C. Cheng, and D. Kohli, 1994. "Synthesis of six-link, slider-crank and four-link mechanisms for function, path and motion generation using homotopy with m-homogenization," *Journal of Mechanical Design*, 116(4):1122–1131.

[30] Z. Luo and J. S. Dai, 2007. "Patterned bootstrap: A new method that gives efficiency for some precision position synthesis problems," *Journal of Mechanical Design*, 129(2):173–183.

[31] M. Plecnik and J. M. McCarthy, 2015. "Computational Design of Stephenson II Six-bar Function Generators for 11 Accuracy Points," under review for the ASME *Journal of Mechanisms and Robotics*, March 2015.

[32] S. K. Banala and S. K. Agrawal, 2005. "Design and optimization of a mechanism for out-of-plane insect winglike motion with twist," *Journal of Mechanical Design*, 127(4):841–844.

[33] M. McDonald and S. K. Agrawal, 2010. "Design of a bio-inspired spherical four-bar mechanism for flapping-wing micro air-vehicle applications," *Journal of Mechanisms and Robotics*, 2(2):021012.

[34] P. S. Sreetharan, J. P. Whitney, M. D. Strauss, and R. J. Wood, 2012. "Monolithic fabrication of millimeter-scale machines," *Journal of Micromechanics and Microengineering*, 22(5):055027.

[35] Z. E. Teoh, and R. J. Wood, 2013. "A flapping-wing microrobot with a differential angle-of-attack mechanism," *Robotics and Automation (ICRA), 2013 IEEE International Conference*, 1381–1388.

[36] M. Keennon, A. Andryukov, K. Klingebiel, and H. Won, 2014. "Air vehicle flight mechanism and control method for non-sinusoidal wing flapping," US Patent 2014/0158821 A1.

[37] F. Haas and R. J. Wootton, 1996. "Two basic mechanisms in insect wing folding," *Proceedings of the*

Royal Society of London, Series B: Biological Sciences, 263(1377):1651-1658.

[38] B. Tobalske, and K. Dial, 1996. "Flight kinematics of black-billed magpies and pigeons over a wide range of speeds," *The Journal of Experimental Biology*, 199(2):263–280.

[39] B. W. Tobalske, N. E. Olson, and K. P. Dial, 1997. "Flight style of the black-billed magpie: variation in wing kinematics, neuromuscular control, and muscle composition," *Journal of Experimental Zoology*, 279(4):313–329.

[40] J. M. McCarthy and G. S. Soh, 2010. *Geometric Design of Linkages*, 2nd ed, Springer.

[41] M. D. Greenberg, 1988. *Advanced Engineering Mathematics*, Prentice-Hall.

[42] N. S. Proctor, 1993. *Manual of Ornithology: Avian Structure & Function*, Yale University Press.

[43] E. A. Dijksman, 1976. *Motion Geometry of Mechanisms*, Cambridge University Press, London.